*remote sensing*

MDPI

*Article*

# Climate Variability and Groundwater Levels: A Correlation and Causation Analysis

**Fabian J. Zowam and Adam M. Milewski ***

Department of Geology, University of Georgia, Athens, GA 30602, USA; fabianzowam@uga.edu
* Correspondence: milewski@uga.edu

## Highlights

### What are the main findings?

- There may be a moderate to strong, lagged relationship between terrestrial water cycle intensity and groundwater levels in semi-arid to arid climates, based on findings in Arizona, USA.
- In Arizona, the relationship was dominantly negative where it occurred, with terrestrial water cycle intensity responding 1–2 months after groundwater level changes. It also showed close associations with Active Management Areas (AMAs), where the state enforces the strictest groundwater regulations due to persistent overdraft concerns.

### What are the implications of the main findings?

- The nature of this trend implies that an intensified water cycle today may signal an already depleting groundwater resource at the affected locations.
- This backward interpretation could help determine when immediate management responses and swift interventions are necessary.

## Abstract

Short-term fluctuations in climate patterns (climate variability) often indicate long-term climate change (CC) trends, which are a global threat to our planet today. CC is speeding up the terrestrial water cycle and potentially affecting groundwater availability, a major component of that cycle. Considering that terrestrial water cycle intensity (WCI) and groundwater level (GWL) are indicators of CC and groundwater availability, respectively, this study explored the dynamic relationship between WCI and GWL anomalies (WCIAs and GWLAs, respectively) in an arid region, based on an innovative approach to statistical correlation and causation analysis. Pearson correlation (r) assessed the strength and direction of a contemporaneous linear relationship between both variables; a cross-correlation function (CCF) determined the dynamic nature of those relationships considering monthly lags up to a predetermined maximum of 12 months; and Granger causality (GC) tests assessed the statistical significance of past values of the lead variable in enhancing the prediction of future values of the lagged variable. A contemporaneous linear relationship between both variables was mostly absent but appeared at various lags. At these lags, the strongest correlations were dominantly negative, with GWLA leading WCIA, as supported by the GC tests. This trend suggests that the intensification of the water cycle reflects a decline in past groundwater levels, necessitating immediate water management actions in the affected areas.

Check for updates

Academic Editor: Teodosio Lacava

Received: 4 December 2025
Revised: 27 February 2026
Accepted: 9 March 2026
Published: 19 March 2026

**Copyright:** © 2026 by the authors. Licensee MDPI, Basel, Switzerland. This article is an open access article distributed under the terms and conditions of the Creative Commons Attribution (CC BY) license.

**Keywords:** climate variability; climate change; water cycle; groundwater

## 1. Introduction

Climate change (CC), according to the Intergovernmental Panel on Climate Change (IPCC), is the statistically significant variation in average weather conditions lasting for decades or longer [1]. It is a global menace today, driven largely by human activities that release greenhouse gases into the atmosphere, altering global temperature and precipitation patterns [1–3]. Climate variability (CV), on the other hand, refers to short-term fluctuations associated with CC [4]. Initially, it described the fluctuations due to natural processes, but is now understood to reflect the anthropogenic influences that define CC [4,5], and is therefore sometimes referred to as CC [5].

Hydrogeologists are concerned about the impacts of climate variability and change on groundwater (GW) resources [6–10]. These impacts could be direct or indirect, where direct impacts generally affect its quantity and indirect impacts affect the quality. Specifically, direct impacts involve the natural replenishments or recharge and directly affect the availability of the resource [9]. Indirect impacts may include alterations in GW chemistry [11], increased mobility of geogenic contaminants [12], and leaching of water-soluble contaminants [13] following intense and frequent precipitation events. Additionally, during droughts, and as a result of altered redox conditions of aquifers, environmental pollutants such as nitrates and sulphates may be mobilized [12]. In coastal areas, these impacts include saltwater intrusion due to reduced precipitation and GW recharge [1,14], and seawater flooding due to increased frequency and intensity of large coastal storms, causing sea levels to rise [15]. In general, CC is causing alterations to key aspects of GW quality through variations in concentrations of organic and inorganic compounds, dissolved oxygen levels, salinity, and pH [16].

Effectively managing GW resources now requires the inclusion of CC and variability impact assessments, which have previously been overlooked [17,18]. Scientists at the U.S. Geological Survey (USGS) work with various tiers of national partners and international collaborators to understand how these factors impact groundwater availability in the United States [17]. However, because variations in climate patterns may mean that broad generalizations do not adequately capture these interactions, there is a need for more localized studies that provide specific insights into how these variations impact GW. At the same time, arid regions are environmentally fragile and highly sensitive to global climate variability and change, making climate assessments in these regions a hot topic in the climate science field [19]. Given this context, this study assesses local CV–GW interactions in an arid region in the contiguous United States, with a focus on impacts related specifically to GW availability.

In examining these interactions, it is important to consider the following: (1) natural GW availability depends largely on precipitation, which is a major component of the global water cycle, i.e., a dynamic system describing the continuous movement and exchange of water between the Earth's surface and atmosphere. (2) Climate variability has significant direct impacts on this system [20,21]. With extreme weather becoming even more extreme, the disparity in precipitation between wet and dry areas is expected to intensify [16]. (3) These changes or shifts in the water cycle over any landscape or terrain can be quantified using the terrestrial water cycle intensity (WCI) metric [22–24].

WCI represents the intensification of the water cycle in the sense of an acceleration of the land–atmosphere water exchange. Huntington et al. (2018) [23] defined this phenomenon as the sum of precipitation (P) and evapotranspiration (ET) over a given

landscape unit and time interval. The authors went further to calculate the WCI for the contiguous United States (CONUS) between 1945 and 2014, using ground-based P and ET measurements [23]. In a recent study, Zowam et al. (2023) [24] validated the use of remote sensing for the WCI computation and extended the calculations for the CONUS to cover a more recent period (2001 to 2019). As reported in their study, the water cycle may be speeding up across the CONUS, particularly the West, driven by increases in both P and ET [24]. Arizona showed the strongest intensities among arid areas in the region, based on the difference between the 2010–2019 and 2001–2009 WCI averages, attributable to simultaneous increases in both P and ET [24].

Using satellite-based estimates of P and ET for the WCI estimation, along with groundwater level (GWL) measurements from 59 monitoring wells across Arizona (Figure 1), we explored the dynamic relationship between WCI and GWL anomalies at the locations of those wells, employing an innovative approach to statistical correlation and causation analyses. We hypothesize that (1) monthly WCI and GWL anomalies over Arizona, between January 2010 and December 2019, show a strong, negative correlation. (2) There is a strong lead–lag relationship between both variables, where the lead variable (WCI anomaly) improves the prediction of the lag variable (GWL anomaly).

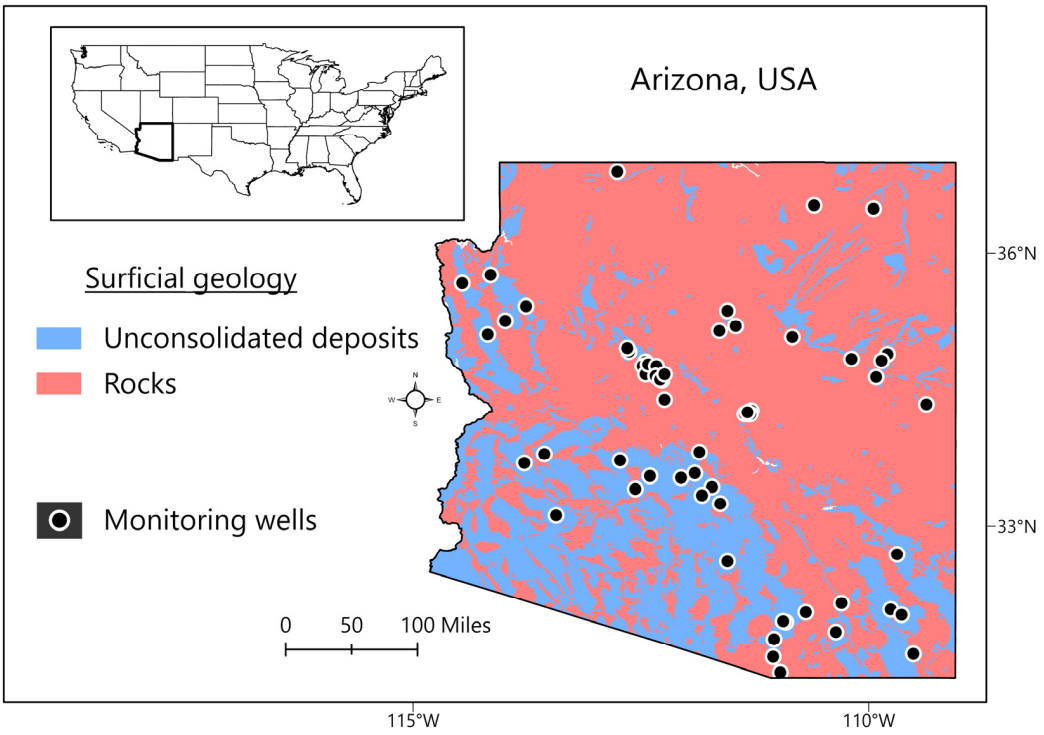


**Figure 1.** Study area showing groundwater monitoring wells and surficial geology. Modified from Zowam and Milewski (2024) [25], which predicted GWL changes at ungauged locations across the study area (at a grid size of 0.125° × 0.125°) using the same well data as this study.

## 2. Materials and Methods

The data and statistical methods employed in this study are described below:

### *2.1. Ground-Based Data*

Daily GWL observations from 59 monitoring wells (Figure 1) were downloaded from the National Groundwater Monitoring Network (NGWMN) data portal (https://cida.usgs.gov/ngwmn/index.jsp, accessed on 29 January 2023), and aggregated to monthly averages, to ensure temporal alignment with the WCI rasters (introduced in the next subsection). Of the 59 wells, 38 were drilled into unconsolidated material (sand and gravel) aquifers

and 21 into consolidated rocks (Figure 1) [25]. The monthly data showed varying seasonal signatures, including persistent increases and declines; early-, mid-, and late-year recoveries and declines; and smooth, unimodal oscillatory patterns, all suggesting heterogeneous controls on GWLs in the region (Figure 2).

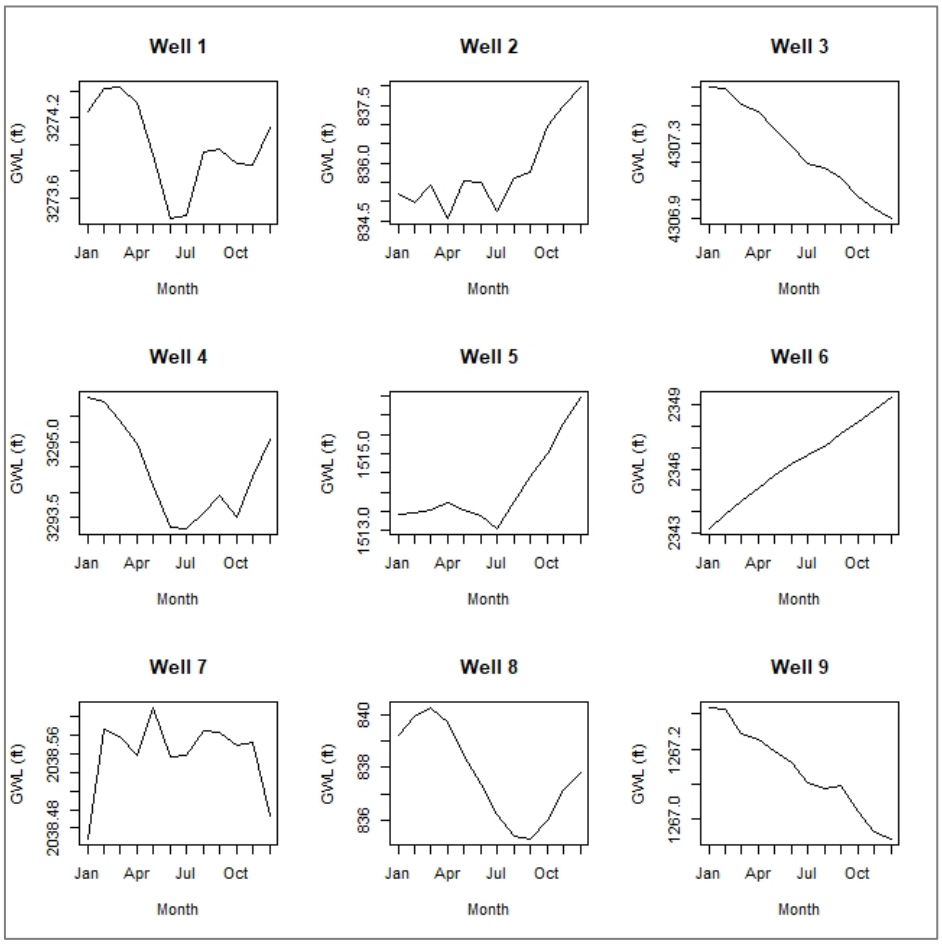


**Figure 2.** Monthly GWL variability across monitoring wells. Only the first nine well locations are shown. All nine wells were drilled into unconsolidated material aquifers.

### *2.2. Satellite-Based Data*

Precipitation measurements from space began in 1997 with the Tropical Rainfall Measuring Mission (TRMM) [24]. Its immediate successor, the Global Precipitation Measurement (GPM) mission, offered significant improvements in terms of latitudinal coverage and resolution, and quantified precipitation more accurately [24,26,27]. We utilized the final processing run of the GPM dataset generated using the Integrated Multi-Satellite Retrievals for the GPM (IMERG) algorithm. IMERG provides precipitation estimates at a spatial resolution of 0.1° × 0.1° and temporal resolution of 30 min [26,27], and is considered an excellent alternative to ground-based observations [26]. It is also particularly effective over arid and semi-arid regions [27,28]. The monthly averaged 0.1° × 0.1° resolution dataset was downloaded from the NASA data portal (https://gpm.nasa.gov/data/directory, accessed on 11 May 2021).

For ET, a finer grid resolution (0.01° × 0.01°) synthesizing various global satellite ET measurement efforts was downloaded from the Harvard Dataverse repository (https://doi.org/10.7910/DVN/ZGOUED, accessed on 3 July 2021). This product was generated by evaluating and ranking the performance of twelve global satellite ET products against high-quality flux eddy covariance ground observations, based on several metrics and

validation criteria [24,29]. The best-performing datasets were combined into a monthly ET ensemble product, available from 1982 to 2019, and for land cover types [24,29]. This synthesized product outperformed local ET products in the United States, China, and the continent of Africa [29].

Monthly precipitation and ET rasters at varying grid sizes (Table 1) covering 10 years (2010–2019) were downloaded from their respective data portals and resampled to a 0.125° × 0.125° grid size. This would ensure consistency with the Zowam and Milewski (2024) [25] study that produced gridded GWL anomaly predictions for ungauged locations in the same study area, and allow for the direct integration of hydrogeological assessment in the region. Monthly WCI rasters were derived by simply summing respective precipitation and ET rasters. Unlike GWLs, the monthly WCI data showed consistent seasonal patterns across the network, with peak intensification occurring during summer months (Figure 3).

**Table 1.** Summary of variables used in the study.

| ID | Variable | Type | Resolution | Unit |
|---|---|---|---|---|
| 1 | P | Grid | 0.1° \| monthly | mm |
| 2 | ET | Grid | 0.01° \| monthly | mm |
| 3 | GWL | Point | — \| daily | feet |

P = Precipitation; ET = Evapotranspiration; GWL = Groundwater level. P and ET were resampled to 0.125° × 0.125° and summed to obtain WCI rasters.

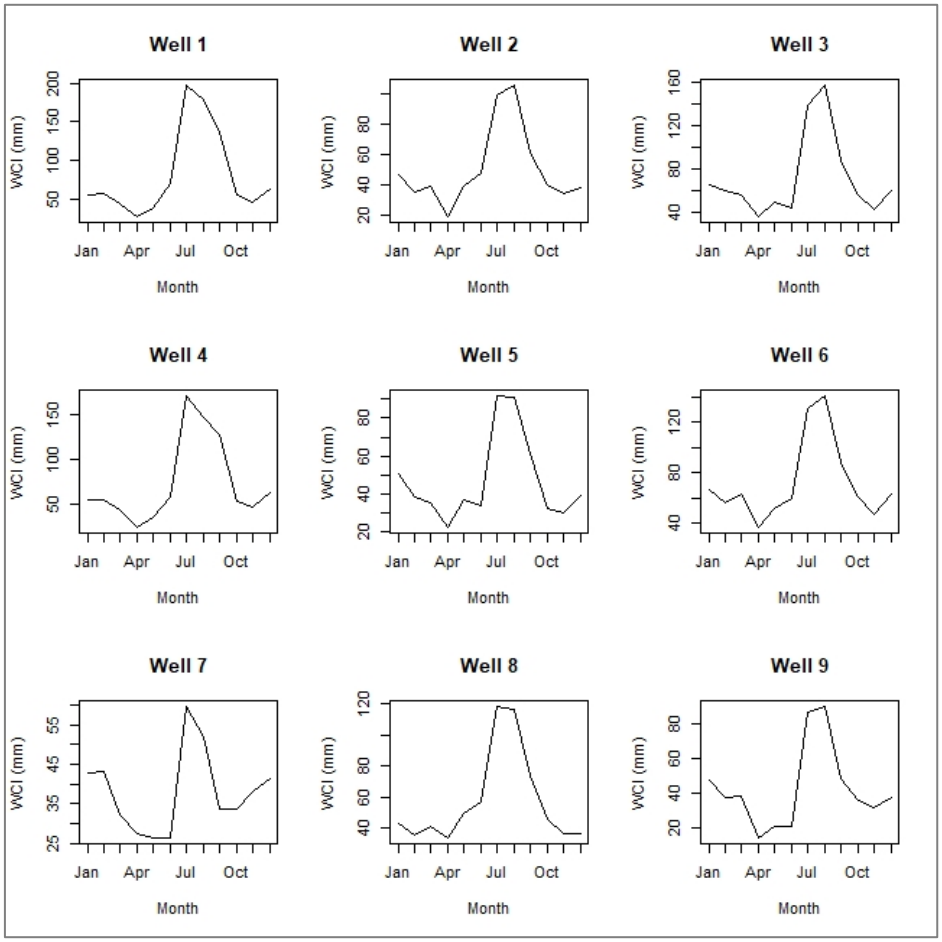


**Figure 3.** Monthly WCI variability across monitoring wells. Only the first nine well locations are shown.

### 2.3. Anomaly Derivation Approach

Monthly WCI and GWL data from January 2010 to December 2019 were obtained as gridded values (WCI) and point-based observations within each grid cell (GWL). The WCI anomaly (WCIA) at each cell was computed as the difference between the monthly value and the ten-year (2010–2019) mean for that cell, as shown below:

$$WCIA_i = WCI_i - \overline{WCI} \quad (1)$$

where $i$ represents monthly time steps from 1 to 120 months (January 2010 to December 2019), and $\overline{WCI}$ is the mean $WCI$ value for a given cell.

Similarly, GWL anomaly (GWLA) was computed as the difference between monthly GWL values and the mean value at each monitoring well location, as shown below:

$$GWLA_i = GWL_i - \overline{GWL} \quad (2)$$

where $i$ represents monthly time steps from 1 to 120 months (January 2010 to December 2019), and $\overline{GWL}$ is the mean $GWL$ value at a given monitoring well location.

Our WCI and GWL anomaly derivation approach is consistent with common practice in hydroclimatology, and has been used in various studies and operational research products [25,30–32], including NASA's GRACE (Gravity Recovery and Climate Experiment) TELLUS project [32], which provides gridded monthly surface mass anomalies as the difference between each month's value and the January 2004 to December 2009 mean.

The relationship between GWL and WCI anomalies was evaluated at the monitoring well locations using WCI data from grids spatially matched to those locations. In cases where multiple wells were located within the same WCI grid, only GWL anomalies would vary. The relationship was also expected to reflect local hydrogeological conditions, including aquifer properties and localized pumping influences; meaning that spatial proximity alone was not sufficient to guarantee identical WCI–GWL relationships.

### 2.4. Statistical Correlation

Differencing both datasets (WCI and GWL anomaly) eliminated any existing time correlation and reduced the number of observations by one. It is a standard practice in time-series analysis for removing or reducing the effects of complicating data characteristics, including trends, autocorrelation, and periodicity [33,34]. Based on visual inspections of the time-series plots and results of Augmented Dickey–Fuller (ADF) tests, we successfully removed trends and achieved stationarity. The differenced time series also satisfied the assumptions for Pearson correlation, following assessments based on strip charts, histograms, and bivariate plots, while considering only substantial departures from normality. Pearson correlation was performed simultaneously on 59 grids, each corresponding to the location of a monitoring well, to determine the strength and direction of the linear relationship between the variables (r), expressed mathematically as:

$$r_{XY} = \frac{\sum (X_i - \overline{X})(Y_i - \overline{Y})}{\sqrt{\sum (X_i - \overline{X})^2 \sum (Y_i - \overline{Y})^2}} \quad (3)$$

where $r_{XY}$ is the Pearson correlation coefficient between the variables $X$ and $Y$, which ranges from $-1$ (perfect negative) to +1 (perfect positive); $X_i$ and $Y_i$ are individual observations of variables $X$ and $Y$, respectively; $\overline{X}$ is the mean of variable $X$; $\overline{Y}$ is the mean of variable $Y$ [35].

The statistical correlation described above assumes a contemporaneous relationship between WCI and GWL anomalies, which may not necessarily be the case. Thus, we

repeated the correlations at several lag intervals, up to a predetermined maximum of 12 months, aligning with the natural annual window for monthly data. This approach is known as cross-correlation and examines whether the fluctuations in one variable precede, are led by, or occur contemporaneously with fluctuations in the other variable [36]. The result of the cross-correlation function (CCF) analysis is a plot of correlation coefficients at the various examined lags, where the $x$-axis represents lag intervals, and the $y$-axis indicates the correlation coefficients. The $x$-axis extends equally in both positive and negative directions from zero, meaning that a maximum lag of 12 months, for example, will show correlation coefficients at 24 different lags (−12 to +12). Considering how the analysis was set up, substantial correlation coefficients at negative lags indicate that the input time series precedes the output series, and vice–versa [37]. In our setup, WCI anomaly (WCIA) is the input variable, and GWL anomaly (GWLA) is the response variable of interest.

Statistical correlation quantifies the relationship (strength, direction) between any two variables, and also serves as a diagnostic tool for different purposes, including anomaly detection in time series data (based on deviations from expected relationships) [38], and feature selection in predictive modeling and machine-learning applications [39,40]. In addition to assessing the linear relationships between WCIA and GWLA at various lags, we used correlation to identify candidate well locations and lags for Granger causality (GC) tests.

### *2.5. Granger Causality*

First introduced by Clive W.J. Granger, GC is a statistical concept used to investigate causal relations between stationary time series of two or more variables [41]. It was originally applied in the field of economics [41], but has been extended to various other disciplines, including atmospheric and climate sciences [42,43], environmental sciences [44–47], and, recently, hydrogeology to understand groundwater patterns [48].

Singh and Borrok (2019) [48] conducted the first GC analysis to identify the causes of long-term groundwater patterns, focusing on climate and agricultural drivers. Since then, various other applications have emerged. Kim et al. (2023) [49] used it to select hydrologic and meteorological predictors for machine-learning-based GWL forecasting in an area; Le et al. (2021) [50] focused on the influence of precipitation variability on GWLs; Gomes Calixto et al. (2021) [51] used it to evaluate interactions between water budget components (P, ET, streamflow, and GWL) at a relatively small watershed; Zhang et al. (2023) [52] applied it to quantify the effects of P and GW extraction on GWLs for a much larger watershed. In a different type of application, Yee and Choi (2022) [53] used it to determine whether an earthquake approximately 17 miles from a site had any influence on GWLs at the site.

Given two stationary time-series $X$ and $Y$, we say that $X$ Granger-causes $Y$ if our ability to predict future values of $Y$ is enhanced by using all information except current values of $X$ [41,48]. This is expressed mathematically as:

$$X_t = \sum_{j=1}^{m} a_j X_{t-j} + \sum_{j=1}^{m} b_j Y_{t-j} + \in_t \quad (4)$$

And [41]

$$Y_t = \sum_{j=1}^{m} c_j X_{t-j} + \sum_{j=1}^{m} d_j Y_{t-j} + n_t \quad (5)$$

where $X_t$ and $Y_t$ are two stationary time series; $j$ is the current lag; m is the maximum number of lags considered; $a_j$, $b_j$, $c_j$ and $d_j$ are coefficients; and $\in_t$ and $n_t$ represent the two uncorrelated white noise series [41]. $X_t$ will Granger-cause $Y_t$ if $c_j$ is not zero [41]. Similarly, $Y_t$ will Granger-cause $X_t$ if $b_j$ is not zero [41]. If both events occur simultaneously then a feedback relationship exists between both variables [41]. This is known as bidirectional Granger causality [54–56].

GC tests were conducted on the significant lags identified in the CCF analysis, evaluating the contribution of past values of one time series in predicting future values of another (Figure 4). The null hypothesis that the past values of WCIA do not provide any useful information for predicting GWLA (and vice versa) was tested. The hypothesis for each test was rejected when a *p*-value less than 0.05 was returned.

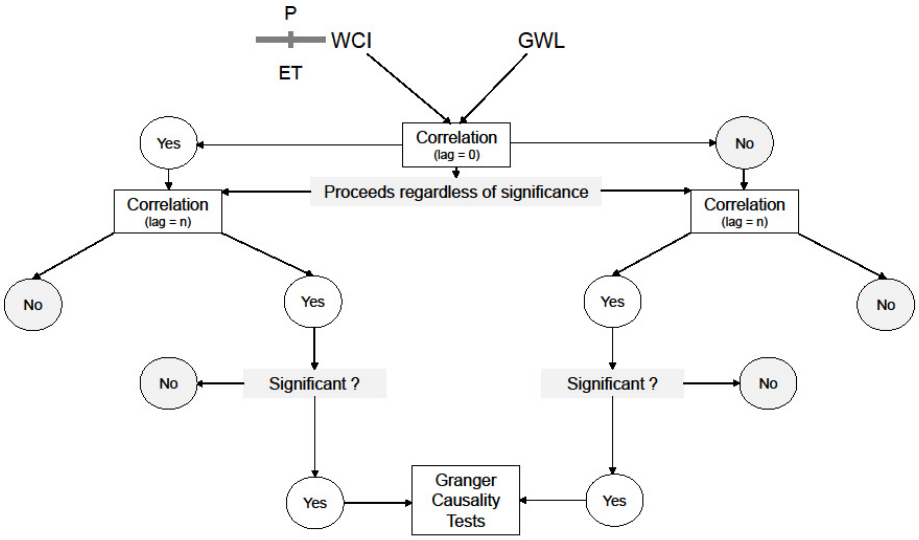


**Figure 4.** Methodological flow chart. Regardless of the outcome of the correlation at zero lag or its statistical significance, we repeated the process for lag = n months, where n is 12. Significance is evaluated using a 95% confidence interval threshold.

## 3. Results

All analyses were carried out in R (version 4.1.1). Statistical correlations were conducted at each monitoring well location, first at zero lags and then at lags up to 12 months (−12 to +12). The results show the correlation coefficients at zero lag, the maximum correlation coefficient (across all lags) and its corresponding lag, and an assessment of the statistical significance of the reported correlation coefficients (Table 2). Coefficients are normally distributed and considered statistically significant when they exceed the 95% confidence interval threshold, indicating that the observed correlation is unlikely due to random chance if the null hypothesis is true [57]. Well locations with the highest correlation (Max Cor) were selected as candidates for the GC tests (Figure 5).

**Table 2.** Summary of correlation analysis at all monitoring well locations. 'Cor' refers to the correlation coefficient, and 'Max Cor' refers to the maximum correlation coefficient considering all lags. Negative (−ve) lags at the Max Cor suggest that WCIA precedes GWLA, while positive (+ve) lags indicate the reverse.

| ID | Cor (Lag = 0) | Significant? (Lag = 0) | Max Cor | Lag (Max Cor) | Significant? (Max Cor) |
|---|---|---|---|---|---|
| 1 | −0.07 | No | +0.45 \| −0.44 | −1 \| +1 | Yes |
| 2 | +0.03 | No | −0.23 | −11 | Yes |
| 3 | −0.09 | No | −0.20 | −3 | Yes |
| 4 | +0.08 | No | −0.33 | −10 | Yes |
| 5 | −0.25 | Yes | −0.25 | 0 | n/a |
| 6 | +0.00 | No | +0.12 | +3 | No |
| 7 | −0.07 | No | +0.22 | +2 | Yes |
| 8 | −0.16 | No | +0.29 | +4 | Yes |
| 9 | −0.26 | Yes | +0.35 | +1 | Yes |
| 10 | +0.19 | Yes | −0.27 | +1 | Yes |

**Table 2.** *Cont.*

| ID | Cor (Lag = 0) | Significant? (Lag = 0) | Max Cor | Lag (Max Cor) | Significant? (Max Cor) |
|---|---|---|---|---|---|
| 11 | −0.10 | No | −0.26 | −11 | Yes |
| 12 | +0.09 | No | +0.25 | −6 | Yes |
| 13 | −0.09 | No | +0.30 | +7 | Yes |
| 14 | +0.12 | No | −0.44 | +1 | Yes |
| 15 | +0.05 | No | −0.25 | −3 | Yes |
| 16 | −0.21 | Yes | +0.27 | +3 | Yes |
| 17 | −0.02 | No | +0.26 | −3 | Yes |
| 18 | +0.03 | No | −0.26 | −2 | Yes |
| 19 | −0.07 | No | +0.21 | +4 | Yes |
| 20 | −0.03 | No | −0.24 | +1 | Yes |
| 21 | +0.05 | No | −0.32 | +1 | Yes |
| 22 | −0.38 | Yes | −0.38 | 0 | n/a |
| 23 | +0.03 | No | +0.32 | 8 | Yes |
| 24 | −0.06 | No | −0.38 | 1 | Yes |
| 25 | +0.19 | Yes | +0.19 | 0 | n/a |
| 26 | −0.37 | Yes | −0.37 | 0 | n/a |
| 27 | −0.08 | No | +0.17 | +7 | No |
| 28 | −0.15 | No | +0.37 | +6 | Yes |
| 29 | −0.19 | Yes | +0.45 | −5 | Yes |
| 30 | +0.23 | Yes | −0.24 | −4 | Yes |
| 31 | −0.20 | Yes | −0.37 | +7 | Yes |
| 32 | +0.02 | No | +0.21 | +10 | Yes |
| 33 | −0.00 | No | −0.60 | +1 | Yes |
| 34 | −0.17 | No | −0.17 | 0 | n/a |
| 35 | −0.24 | Yes | +0.25 | +3 | Yes |
| 36 | +0.00 | No | −0.22 | −9 | Yes |
| 37 | −0.01 | No | +0.24 | +11 | Yes |
| 38 | −0.05 | No | +0.23 | +8 | Yes |
| 39 | −0.07 | No | +0.29 | −7 | Yes |
| 40 | −0.12 | No | +0.19 | +3 | Yes |
| 41 | +0.09 | No | −0.42 | +2 | Yes |
| 42 | −0.11 | No | −0.26 | −2 | Yes |
| 43 | +0.12 | No | −0.43 | +1 | Yes |
| 44 | −0.07 | No | +0.31 | +3 | Yes |
| 45 | −0.15 | No | −0.29 | −6 | Yes |
| 46 | −0.12 | No | −0.26 | −6 | Yes |
| 47 | −0.11 | No | −0.31 | 1 | Yes |
| 48 | −0.05 | No | −0.35 | 1 | Yes |
| 49 | −0.35 | Yes | −0.35 | 0 | n/a |
| 50 | +0.18 | No | −0.42 | +1 | Yes |
| 51 | −0.31 | Yes | +0.38 | −8 | Yes |
| 52 | −0.14 | No | −0.33 | −12 | Yes |
| 53 | −0.19 | Yes | −0.26 | +12 | Yes |
| 54 | −0.16 | No | +0.36 | −9 | Yes |
| 55 | +0.05 | No | +0.15 | +10 | No |
| 56 | +0.06 | No | +0.24 | −6 | Yes |
| 57 | −0.15 | No | −0.35 | +7 | Yes |
| 58 | +0.03 | No | +0.31 | −4 | Yes |
| 59 | −0.06 | No | −0.20 | −2 | Yes |

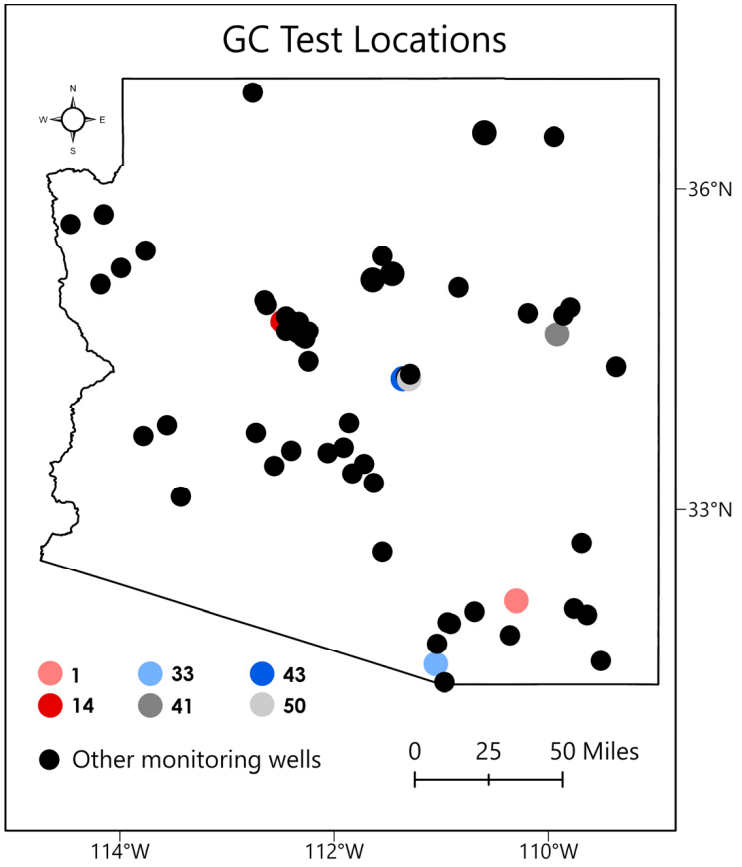


**Figure 5.** Location of the GC test wells. The strongest correlations occurred at the locations of the colored circles. Wells 1 and 33 were drilled into unconsolidated material aquifers, and wells 14, 41, 43, and 50 were drilled into rock aquifers.

At the GC test well locations (as in most cases), the variables were not contemporaneously correlated since the maximum correlation occurred at non-zero lags (Figure 6).

GC tests are forward-looking time-series analyses that determine whether past values of a predictor variable are useful for predicting current values of the target variable beyond the information obtained from past values of the target variable themselves. Based on the *p*-values (Table 3) and a 5% significance level, we reject the null hypothesis that past values of GWLA do not contain useful information for predicting WCIA values at all six wells. Similarly, we reject the null hypothesis that past values of WCIA do not contain useful information for predicting GWLA values at wells 1 and 33, where bidirectional causality may be occurring (Table 3).

**Table 3.** Results of the GC tests conducted at well locations with the strongest lagged correlation coefficients. WCIA~GWLA implies that GWLA is treated as the independent variable, as determined by the CCF analysis for the respective wells. GWLA~WCIA implies that WCIA is treated as the independent variable, to evaluate the presence of bidirectional causality.

| ID | Lag (Max Cor) | *p*-Value (WCIA~GWLA) | *p*-Value (GWLA~WCIA) |
|---|---|---|---|
| 1 | +1 | 0.000000062 | 0.000000053 |
| 14 | +1 | 0.0000016 | 0.827 |
| 33 | +1 | 0.00000000000038 | 0.001 |
| 41 | +2 | 0.0000000065 | 0.148 |
| 43 | +1 | 0.0000012 | 0.08 |
| 50 | +1 | 0.0000054 | 0.06 |

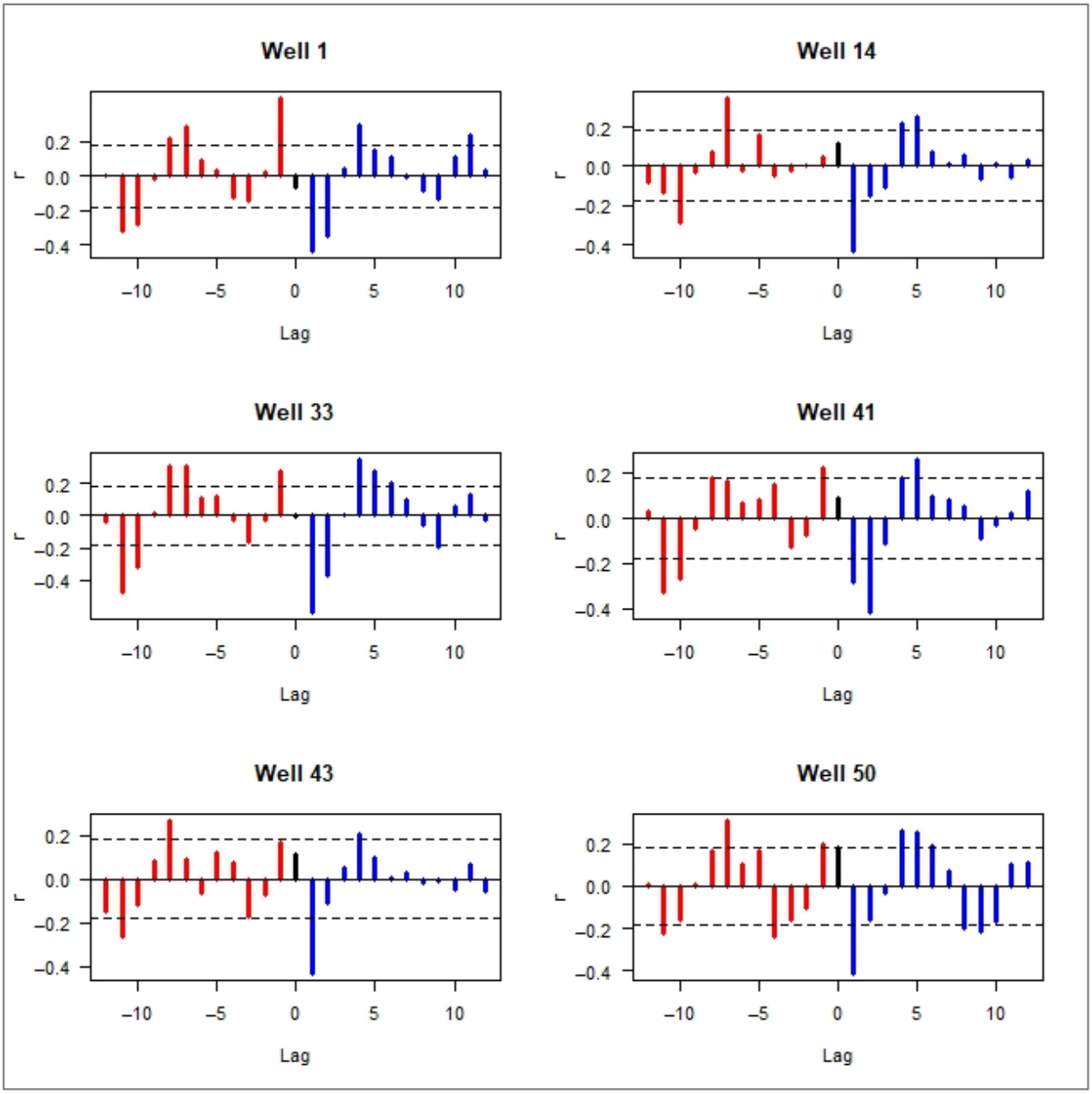


**Figure 6.** CCF plot for representative well locations. Negative lags (red) suggest that WCIA precedes GWLA, and positive lags (blue) show GWLA preceding WCIA. The correlation at zero lag is shown in the solid black line, and the black dotted lines represent the lower and upper confidence limits beyond which a correlation coefficient (*y*-axis) is statistically significant. Wells 1 and 33 were drilled into unconsolidated material aquifers, and wells 14, 41, 43, and 50 were drilled into rock aquifers.

Some of the GC test wells showed a close association with Active Management Areas (AMAs) (Figure 7). AMAs are areas experiencing groundwater overdraft issues due to their strong reliance on groundwater, prompting the active management of the resource [58]. For instance, the relationship between WCIA and GWLA is particularly notable at well 33, as indicated by the results of the correlation analysis (Table 2), GC tests (Table 3), its association with an AMA (Figure 7), and the scatter plots of contemporaneous and lagged correlations (Figure 8).

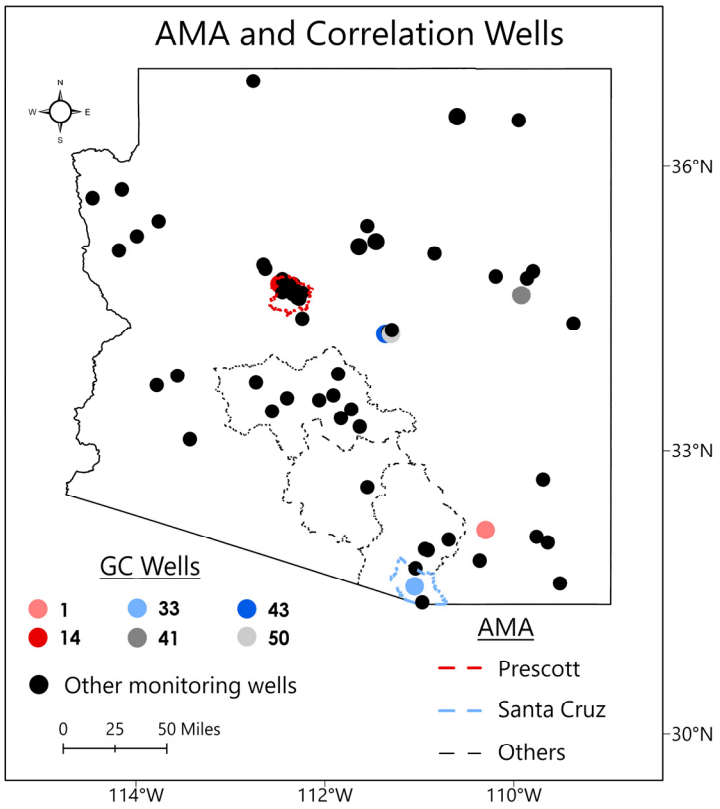


**Figure 7.** AMAs and correlation wells. The GC test wells (colored circles) represent the locations of the largest correlation coefficients in the study area. Some of these wells were located within AMAs (Prescott and Santa Cruz). wells 1 and 33 were drilled into unconsolidated material aquifers, and wells 14, 41, 43, and 50 were drilled into rock aquifers.

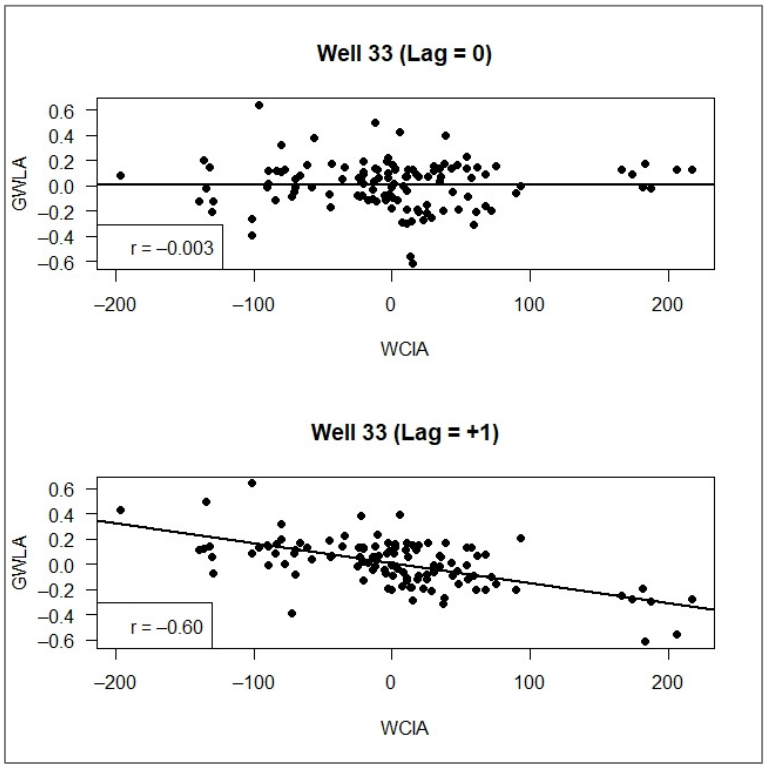


**Figure 8.** Scatter plots for well 33 illustrate contemporaneous (lag = 0) and lagged (lag = +1) relationships between WCI and GWL anomalies. Well 33 was drilled into an unconsolidated material aquifer.

## 4. Discussion

The relationship between GWLs and driving factors is complex and nonlinear [25,59–62], but if precipitation is typically linearly correlated with GWL [63–65], likewise ET [65], we expect the WCI, a variable obtained from precipitation and ET, to also show a linear relationship with GWL, reflecting the dominant of the two variables. This was mostly not the case for the contemporaneous relationship (lag = 0) between GWLA and WCIA examined in this study. However, a moderate to strong linear relationship was observed at six monitoring well locations (1, 14, 33, 41, 43, and 50) when WCIA at time t + k was compared with GWLA, where k represents the lag (Table 2). This correlation occurred at positive lags, implying that changes in WCIA lagged GWLA, and was negative at all six sites, indicating that an increase in lagged values of WCIA corresponds to a decrease in GWLA values, and vice versa (Table 2). Similar patterns have been reported between groundwater levels and other hydroclimatic indicators, including streamflow changes [66,67] and vegetation health [68]. In semi-arid regions, shallow groundwater has been found to exert a leading control on soil moisture (SM), sustaining wet or dry SM anomalies even after the events that caused them have passed [69]. The control on SM may be depth-dependent, where the strongest coupling may occur at intermediate depths rather than at exclusively shallow or deep groundwater depths [70]. The findings in this study corroborate some of these known interactions and present a new outlook for climate variability and groundwater relationships in the study area.

Contemporaneous correlation (lag = 0) was observed at wells 5, 22, 25, 26, 34, and 49 (Table 2), because at those wells, the maximum correlation appeared at zero lag, indicating that the relationship between the two variables was observed within the same time period (without any delay or time lag between them). This correlation was not significant at well 34, and at wells 5 and 25, it was the only statistically significant correlation. Therefore, at wells 5 and 25, we accept the null hypothesis that there is no significant lead–lag relationship between both variables at the examined lags. Also, the maximum correlations at non-zero lags were not statistically significant at wells 6, 27, and 55 (Table 2). At these wells (as well as at well 34), there is no evidence of a relationship between WCIA and GWLA.

The strongest lagged correlation (−0.60) was observed at well 33 (Table 2) and occurred at a lag of +1, indicating that GWLA in the current month had a strong linear relationship with WCIA in the following month (and vice versa). GWLA also showed the strongest relationships with precipitation (−0.58) and evapotranspiration (−0.43) anomalies, all three occurring at the same lag (+1), suggesting that the influence of GWL on climate at that location occurs at a lag of +1. GC tests returned statistically significant results at all six wells based on *p*-values (Table 3), implying that the past values of GWLA provide useful information for predicting WCIA values beyond what is provided by the autoregressive structure of the WCIA variable. But at wells 1 and 33, WCIA also provided useful information for predicting GWLA (Table 3). This suggests that bidirectional Granger causality exists at those locations (and lag). However, at well 33 specifically, the much larger F-statistic implied stronger evidence for the former (GWLA Granger causing WCIA). F-statistics measure the ratio of explained to unexplained variance in statistical analyses [71], and the corresponding *p*-value represents the probability of observing the statistic or one more extreme, if the null hypothesis is true [34].

Out of the five AMAs—Santa Cruz, Prescott, Phoenix, Pinal, and Tucson [58,72,73]—Prescott and Santa Cruz contained monitoring wells with some of the strongest lagged correlations, including well 33 (Figure 7). This suggests that these AMAs might be hydrogeologically sensitive to shifts in the terrestrial water cycle. The study area may also be experiencing significant GWL interactions with several other factors. The USGS has identified linkages between GW trends, withdrawal rates, and land subsidence in the

Tucson AMA [74,75]. At the affected areas, GWL increases were a direct result of a decrease in withdrawal rates [74,75], suggesting that, perhaps, pumping practices may have exerted a stronger influence on the AMA than WCI changes evaluated in this study. Furthermore, since surface cracks from excessive GW withdrawal were first discovered in Arizona in the early 1950s, GWL declines have continued to result in extensive land subsidence and surface cracking, especially in the southern parts of the state [76]. For example, in the Wilcox basin in southeastern Arizona, GWLs dropped by up to 32.1 m between 2005 and 2014, coinciding with the largest subsidence rate recorded in the state [76]. Land subsidence is the loss of land surface elevation due to the removal of subsurface support [77]. It typically occurs when an aquifer is unable to support overlying load, with variations in GWLs playing an important role in its development [78]. The opposite of subsidence is uplift, where an increase in GWL through recharge or fluid injection expands aquifer volume [78,79]. Within the Phoenix AMA, GWL declines have been associated with withdrawal rates and managed aquifer recharge (MAR), and seem to level off only when pumping reduces and MAR increases [80]. There, increases in GWLs appeared to occur in areas that had access to surface water from the Colorado River for agricultural, municipal, and industrial use [81]. Aquifer recharge from surface water was also a key factor [81]. Variations in effluent discharge or treated wastewater have also been linked to GW deficits, especially in the Santa Cruz AMA and other parts of southern Arizona [82,83]. Treated wastewater is considered an important source of water in southern Arizona, for irrigation, GW recharge through the Santa Cruz River, and supply to schools, parks, and golf courses in the region [84].

Interestingly, unconventional factors are also at play. In a very recent study that assessed the interactions between GW availability, access variables, and contamination risks across GW supply service areas, the authors associated GWL trends in the study area with demographic and socioeconomic characteristics (age, race, gender, and housing occupancy) [85]. Potable water service areas with higher percentages of Black populations coincided with reduced GW availability, while Hispanic-dominated areas were associated with greater availability, based on GWL trends [85]. In Native American-dominated areas, the relationship varied across the study period (2001–2020) [85]. Service areas with higher female populations were associated with reduced GW availability, those with a higher percentage of children under five showed weak positive associations with GWL declines, and in contrast, higher percentage of older population (over 65 years) exhibited positive relationships with GW availability [85]. Renter-occupied housing was associated with improved GW availability, and married-couple households were associated with reduced GWLs [85]. Student housing showed the strongest associations with GWL declines [85].

Our analyses evaluate statistical associations between GWLA and WCIA and do not attribute WCI changes solely to groundwater variability (or vice versa), especially considering that several monitoring wells were located within AMAs, where groundwater stress has been widely reported and associated with multiple factors. Given that several other factors simultaneously influence GWLs across the study area, future work can build on the insights from this study to understand how each factor specifically influences WCI-GWL relationships, especially at AMAs and other vulnerable areas. While WCI can be calculated from satellite-based estimates of precipitation and ET, obtaining good quality GWL data may be challenging due to the impracticality of installing GWL monitoring wells everywhere, which is where predictive models may come in handy. Studies such as Zowam and Milewski (2024) [25], which predicted monthly GWL anomalies across the entire study area using machine-learning and geostatistical interpolation methods, can be a useful resource to extend the statistical framework presented in this study to ungauged sites and incorporate additional variables. Future work must also consider climate projections and population growth patterns. CV affects natural GW recharge, and growth patterns

influence GW extraction and pumping behavior to meet growing domestic, industrial, and agricultural water needs. A combination of both is expected to produce more extreme GW declines [86,87].

## 5. Conclusions

The dynamic relationship between WCIs and GWLs at local scales across the predominantly arid U.S. state of Arizona was evaluated using statistical correlation and causation analyses. Circling back to the hypotheses outlined in the introduction: (1) GWLA did not show a strong negative contemporaneous correlation with WCIA. The correlation was weak or absent, and not necessarily negative, across all wells. (2) Although the study identified a lead–lag relationship between both variables, this relationship was also not strong across all 59 wells, and where it was strong, GWLA generally led WCIA. Therefore, we reject both hypotheses.

The strongest lagged correlations ($r > \pm 0.4$) were dominantly negative across all identified wells. This trend suggests that a continuous intensification of the water cycle reflects a decline in past GWLs in the affected areas. The implication of the nature of this trend is that an intensified water cycle today may signal an already depleting groundwater resource at the affected locations. Although this backward interpretation may not be useful for informing proactive actions, it could help determine when immediate management responses and swift interventions are necessary. Furthermore, the connections with AMAs reinforce the need for continuous monitoring and effective management of groundwater in vulnerable areas.

**Author Contributions:** F.J.Z. was responsible for the conceptualization, methodology, analysis, and original draft preparation. A.M.M. supervised the project and reviewed drafts of the manuscript. All authors have read and agreed to the published version of the manuscript.

**Funding:** This research was supported by the Miriam Watts-Wheeler Research Fund, awarded by the Department of Geology, the University of Georgia.

**Data Availability Statement:** The data presented in this study are available on request from the corresponding author.

**Conflicts of Interest:** The authors declare no conflicts of interest.

## Abbreviations

The following abbreviations are used in this manuscript:

| | |
|---|---|
| AMA | Active management area |
| CC | Climate change |
| CCF | Cross-correlation function |
| CONUS | Contiguous United States |
| CV | Climate variability |
| ET | Evapotranspiration |
| GC | Granger Causality |
| GW | Groundwater |
| GWL | Groundwater level |
| GWLA | Groundwater level anomaly |
| P | Precipitation |
| r | Pearson correlation coefficient |
| USGS | U.S. Geological Survey |
| WCI | Water Cycle Intensity |
| WCIA | Water Cycle Intensity anomaly |

## References


1. Kumar, C.P. Climate change and its impact on groundwater resources. *Int. J. Eng. Sci.* **2012**, *1*, 43–60.
2. Trenberth, K.E. Changes in precipitation with climate change. *Clim. Res.* **2011**, *47*, 123–138. [CrossRef]
3. Trenberth, K.E. Climate change caused by human activities is happening and it already has major consequences. *J. Energy Nat. Resour. Law.* **2018**, *36*, 463–481. [CrossRef]
4. Pisor, A.C.; Touma, D.; Singh, D.; Jones, J.H. To understand climate change adaptation, we must characterize climate variability: Here's how. *One Earth* **2023**, *6*, 1665–1676. [CrossRef]
5. von der Heydt, A.S.; Ashwin, P.; Camp, C.D.; Crucifix, M.; Dijkstra, H.A.; Ditlevsen, P.; Lenton, T.M. Quantification and interpretation of the climate variability record. *Glob. Planet. Change* **2021**, *197*, 103399. [CrossRef]
6. Chen, Z.; Grasby, S.E.; Osadetz, K.G. Relation between climate variability and groundwater levels in the upper carbonate aquifer, southern Manitoba, Canada. *J. Hydrol.* **2004**, *290*, 43–62. [CrossRef]
7. Ndehedehe, C.E.; Adeyeri, O.E.; Onojeghuo, A.O.; Ferreira, V.G.; Kalu, I.; Okwuashi, O. Understanding global groundwater-climate interactions. *Sci. Total Environ.* **2023**, *904*, 166571. [CrossRef]
8. Khan, H.F.; Brown, C.M. Effect of hydrogeologic and climatic variability on performance of a groundwater market. *Water Resour. Res.* **2019**, *55*, 4304–4321. [CrossRef]
9. Taylor, R.G.; Scanlon, B.; Döll, P.; Rodell, M.; Van Beek, R.; Wada, Y.; Longuevergne, L.; Leblanc, M.; Famiglietti, J.S.; Edmunds, M.; et al. Ground water and climate change. *Nat. Clim. Change* **2013**, *3*, 322–329. [CrossRef]
10. Loáiciga, H.A. Climate change and groundwater. *Ann. Assoc. Am. Geogr.* **2003**, *93*, 30–41. [CrossRef]
11. Barbieri, M.; Barberio, M.D.; Banzato, F.; Billi, A.; Boschetti, T.; Franchini, S.; Gori, F.; Petitta, M. Climate change and its effect on groundwater quality. *Environ. Geochem. Health* **2023**, *45*, 1133–1144. [CrossRef] [PubMed]
12. Aziz, Z. *Potential Impacts of Climate Change on Groundwater Quality*; Division of Science and Research, New Jersey Department of Environmental Protection: Trenton, NJ, USA, 2023; 56p. Available online: https://dspace.njstatelib.org/server/api/core/bitstreams/4a64ad2b-981c-4dde-9c26-749c16ec29cf/content (accessed on 7 August 2024).
13. Kløve, B.; Ala-Aho, P.; Bertrand, G.; Gurdak, J.J.; Kupfersberger, H.; Kværner, J.; Muotka, T.; Mykrä, H.; Preda, E.; Rossi, P.; et al. Climate change impacts on groundwater and dependent ecosystems. *J. Hydrol.* **2014**, *518*, 250–266. [CrossRef]
14. Ranjan, P.; Kazama, S.; Sawamoto, M. Effects of climate change on coastal fresh groundwater resources. *Glob. Environ. Change* **2006**, *16*, 388–399. [CrossRef]
15. Cantelon, J.A.; Guimond, J.A.; Robinson, C.E.; Michael, H.A.; Kurylyk, B.L. Vertical saltwater intrusion in coastal aquifers driven by episodic flooding: A review. *Water Resour. Res.* **2022**, *58*, e2022WR032614. [CrossRef]
16. Dao, P.U.; Heuzard, A.G.; Le, T.X.H.; Zhao, J.; Yin, R.; Shang, C.; Fan, C. The impacts of climate change on groundwater quality: A review. *Sci. Total Environ.* **2023**, *912*, 169241. [CrossRef]
17. Gurdak, J.S.; Hanson, R.T.; Green, T.R. *Effects of Climate Variability and Change on Groundwater Resources of the United States*; No. 2009-3074; US Geological Survey: Reston, VA, USA, 2009.
18. Hanson, R.T.; Newhouse, M.W.; Dettinger, M.D. A methodology to assess relations between climatic variability and variations in hydrologic time series in the southwestern United States. *J. Hydrol.* **2004**, *287*, 252–269. [CrossRef]
19. Yan, X.; Cheng, P.; Zhang, Q.; Li, X.; He, J.; Yan, X.; Zhao, W.; Wang, L. Comparisons of climate change characteristics in typical arid regions of the Northern Hemisphere. *Front. Environ. Sci.* **2022**, *10*, 1033326. [CrossRef]
20. Trenberth, K.E. Water cycles and climate change. In *Global Environmental Change*; Freedman, B., Ed.; Springer: Dordrecht, The Netherlands, 2014; Volume 1, pp. 31–37.
21. Malinowski, Ł.; Skoczko, I. Impacts of climate change on hydrological regime and water resources management of the Narew River in Poland. *J. Ecol. Eng.* **2018**, *19*, 167–175. [CrossRef]
22. Bosilovich, M.G.; Schubert, S.D.; Walker, G.K. Global changes of the water cycle intensity. *J. Clim.* **2005**, *18*, 1591–1608. [CrossRef]
23. Huntington, T.G.; Weiskel, P.K.; Wolock, D.M.; McCabe, G.J. A new indicator framework for quantifying the intensity of the terrestrial water cycle. *J. Hydrol.* **2018**, *559*, 361–372. [CrossRef]
24. Zowam, F.J.; Milewski, A.M.; Richards IV, D.F. A Satellite-Based Approach for Quantifying Terrestrial Water Cycle Intensity. *Remote Sens.* **2023**, *15*, 3632. [CrossRef]
25. Zowam, F.J.; Milewski, A.M. Groundwater Level Prediction Using Machine Learning and Geospatial Interpolation Models. *Water* **2024**, *16*, 2771. [CrossRef]
26. Pradhan, R.K.; Markonis, Y.; Godoy, M.R.V.; Villalba-Pradas, A.; Andreadis, K.M.; Nikolopoulos, E.I.; Papalexiou, S.M.; Rahim, A.; Tapiador, F.J.; Hanel, M. Review of GPM IMERG performance: A global perspective. *Remote Sens. Environ.* **2022**, *268*, 112754. [CrossRef]
27. Morsy, M.; Scholten, T.; Michaelides, S.; Borg, E.; Sherief, Y.; Dietrich, P. Comparative analysis of TMPA and IMERG precipitation datasets in the arid environment of El-Qaa plain, Sinai. *Remote Sens.* **2021**, *13*, 588. [CrossRef]
28. Mohammed, S.A.; Hamouda, M.A.; Mahmoud, M.T.; Mohamed, M.M. Performance of GPM-IMERG precipitation products under diverse topographical features and multiple-intensity rainfall in an arid region. *Hydrol. Earth Syst. Sci.* **2020**, *2020*, 1–27.

29. Elnashar, A.; Wang, L.; Wu, B.; Zhu, W.; Zeng, H. Synthesis of global actual evapotranspiration from 1982 to 2019. *Earth Syst. Sci. Data* **2021**, *13*, 447–480. [CrossRef]
30. Agel, L.; Barlow, M.; Collins, M.J.; Douglas, E.; Kirshen, P. Hydrometeorological conditions preceding extreme streamflow for the Charles and Mystic River basins of Eastern Massachusetts. *J. Hydrometeorol.* **2019**, *20*, 1795–1812. [CrossRef]
31. Adam, M.A.; Scheiber-Enslin, S.E.; Ali, K.A. Estimating water storage change from GRACE satellite data over the Breede Water Management Area, Western Cape, South Africa. *Hydrogeol. J.* **2025**, *33*, 2041–2055. [CrossRef]
32. NASA. GRACE TELLUS Data Portal. Available online: https://grace.jpl.nasa.gov/data/get-data/monthly-mass-grids-land/ (accessed on 16 December 2025).
33. Gallagher, C.; Lund, R.; Robbins, M. Changepoint detection in climate time series with long-term trends. *J. Clim.* **2013**, *26*, 4994–5006. [CrossRef]
34. Holland, S. Data Analysis in the Geosciences. Available online: http://strata.uga.edu/8370/lecturenotes/pvaluesConfidenceIntervals.html (accessed on 7 September 2021).
35. Lee Rodgers, J.; Nicewander, W.A. Thirteen ways to look at the correlation coefficient. *Am. Stat.* **1988**, *42*, 59–66. [CrossRef]
36. Jackson, J.C.; Caluori, N.; Abrams, S.; Beckman, E.; Gelfand, M.; Gray, K. Tight cultures and vengeful gods: How culture shapes religious belief. *J. Exp. Psychol. Gen.* **2021**, *150*, 2057. [CrossRef]
37. Box, G.E.; Jenkins, G.M.; Reinsel, G.C.; Ljung, G.M. *Time Series Analysis: Forecasting and Control*; John Wiley & Sons: Hoboken, NJ, USA, 2015; ISBN 978-1-118-67502-1.
38. Li, H.; Wang, X.; Yang, Z.; Ali, S.; Tong, N.; Baseer, S. Correlation-Based Anomaly Detection Method for Multi-sensor System. *Comput. Intell. Neurosci.* **2022**, *1*, 4756480. [CrossRef] [PubMed]
39. Zowam, S.E. A Machine-Learning-Based Method for Optimizing Well Completion Design Under Reservoir Uncertainty for New Gas Wells in the Montney Formation. Ph.D. Thesis, Texas A&M University, College Station, TX, USA, 2025.
40. Hall, M.A. Correlation-Based Feature Selection for Machine Learning. Ph.D. Thesis, University of Waikato, Hamilton, New Zealand, 1999.
41. Granger, C.W. Investigating causal relations by econometric models and cross-spectral methods. *Econom. J. Econom. Soc.* **1969**, *37*, 424–438. [CrossRef]
42. McGraw, M.C.; Barnes, E.A. Memory matters: A case for Granger causality in climate variability studies. *J. Clim.* **2018**, *31*, 3289–3300. [CrossRef]
43. Attanasio, A.; Pasini, A.; Triacca, U. Granger causality analyses for climatic attribution. *Atmos. Clim. Sci.* **2013**, *3*, 515–522. [CrossRef]
44. Papagiannopoulou, C.; Miralles, D.G.; Decubber, S.; Demuzere, M.; Verhoest, N.E.; Dorigo, W.A.; Waegeman, W. A non-linear Granger-causality framework to investigate climate–vegetation dynamics. *Geosci. Model Dev.* **2017**, *10*, 1945–1960. [CrossRef]
45. Kong, D.; Miao, C.; Duan, Q.; Lei, X.; Li, H. Vegetation-Climate Interactions on the Loess Plateau: A Nonlinear Granger Causality Analysis. *J. Geophys. Res. Atmos.* **2018**, *123*, 11–068. [CrossRef]
46. Kumar, V.; Bharti, B.; Singh, H.P.; Topno, A. Assessing the interrelation between NDVI and climate dependent variables by using granger causality test and vector auto-regressive neural network model. *Phys. Chem. Earth Parts A/B/C* **2023**, *131*, 103428. [CrossRef]
47. Ping, W.Y.; Abd Rais, Z.; Ramli, N.; Mohamed Noor, N.; Ul-Saufie, A.Z.; Hamid, H.A.; Mahmad, M.K.N. Granger Causality Analysis of Air Pollutants and Meteorological Parameters. *Environ. Earth Sci. Proc.* **2025**, *33*, 6. [CrossRef]
48. Singh, N.K.; Borrok, D.M. A Granger causality analysis of groundwater patterns over a half-century. *Sci. Rep.* **2019**, *9*, 12828. [CrossRef]
49. Kim, D.; Jang, C.; Choi, J.; Kwak, J. A case study: Groundwater level forecasting of the Gyorae Area in actual practice on Jeju Island using Deep-Learning technique. *Water* **2023**, *15*, 972. [CrossRef]
50. Le, P.V.; Pham, H.V.; Bui, L.K.; Tran, A.N.; Pham, C.V.; Nguyen, G.V.; Tran, P.A. Responses of groundwater to precipitation variability and ENSO in the Vietnamese Mekong Delta. *Hydrol. Res.* **2021**, *52*, 1280–1293. [CrossRef]
51. Gomes Calixto, K.; Vígolo Coutinho, J.; Wendland, E. Causality and Time-Lagged Dependencies at the Watershed Scale. *ESS Open Arch. Eprints* **2021**, *105*, essoar-10505648.
52. Zhang, J.; Dong, D.; Zhang, L. A New Method for Estimating Groundwater Changes Based on Optimized Deep Learning Models—A Case Study of Baiquan Spring Domain in China. *Water* **2023**, *15*, 4129. [CrossRef]
53. Yee, E.; Choi, M. Influence of the Gyeongju earthquake on observed groundwater levels at a power plant. *Water* **2022**, *14*, 3229. [CrossRef]
54. Maziarz, M. A review of the Granger-causality fallacy. *J. Philos. Econ.* **2015**, *8*, 86–105. [CrossRef]
55. Lopez, L.; Weber, S. Testing for Granger causality in panel data. *Stata J.* **2017**, *17*, 972–984. [CrossRef]
56. Chvosteková, M.; Jakubík, J.; Krakovská, A. Granger causality on forward and reversed time series. *Entropy* **2021**, *23*, 409. [CrossRef]

57. Fathian, F.; Fakheri-Fard, A.; Modarres, R.; Van Gelder, P.H.A.J.M. Regional scale rainfall–runoff modeling using VARX–MGARCH approach. *Stoch. Environ. Res. Risk Assess.* **2018**, *32*, 999–1016. [CrossRef]
58. Majumdar, S.; Smith, R.; Conway, B.D.; Lakshmi, V. Advancing remote sensing and machine learning-driven frameworks for groundwater withdrawal estimation in Arizona: Linking land subsidence to groundwater withdrawals. *Hydrol. Process.* **2022**, *36*, e14757. [CrossRef]
59. Haider, A.; Lee, G.; Jafri, T.H.; Yoon, P.; Piao, J.; Jhang, K. Enhancing Accuracy of Groundwater Level Forecasting with Minimal Computational Complexity Using Temporal Convolutional Network. *Water* **2023**, *15*, 4041. [CrossRef]
60. Tao, H.; Hameed, M.M.; Marhoon, H.A.; Zounemat-Kermani, M.; Heddam, S.; Kim, S.; Sulaiman, S.O.; Tan, M.L.; Sa'adi, Z.; Mehr, A.D.; et al. Groundwater level prediction using machine learning models: A comprehensive review. *Neurocomputing* **2022**, *489*, 271–308. [CrossRef]
61. Ardana, P.D.H.; Redana, I.W.; Yekti, M.I.; Simpen, I.N. Groundwater Level Forecasting Using Multiple Linear Regression and Artificial Neural Network Approaches. *Civ. Eng. Archit.* **2022**, *10*, 784–799. [CrossRef]
62. Najafabadipour, A.; Kamali, G.; Nezamabadi-Pour, H. Application of Artificial Intelligence Techniques for the Determination of Groundwater Level Using Spatio–Temporal Parameters. *ACS Omega* **2022**, *7*, 10751–10764. [CrossRef]
63. Hussain, F.; Wu, R.S.; Shih, D.S. Water table response to rainfall and groundwater simulation using physics-based numerical model: WASH123D. *J. Hydrol. Reg. Stud.* **2022**, *39*, 100988. [CrossRef]
64. Zhang, M.; Singh, H.V.; Migliaccio, K.W.; Kisekka, I. Evaluating water table response to rainfall events in a shallow aquifer and canal system. *Hydrol. Process.* **2017**, *31*, 3907–3919. [CrossRef]
65. Yan, S.F.; Yu, S.E.; Wu, Y.B.; Pan, D.F.; Dong, J.G. Understanding groundwater table using a statistical model. *Water Sci. Eng.* **2018**, *11*, 1–7. [CrossRef]
66. Gullacher, A.; Allen, D.M.; Goetz, J.D. Early warning indicators of groundwater drought in mountainous regions. *Water Resour. Res.* **2023**, *59*, e2022WR033399. [CrossRef]
67. Hunter, S.C.; Allen, D.M.; Kohfeld, K.E. Comparing approaches for reconstructing groundwater levels in the mountainous regions of interior British Columbia, Canada, using tree ring widths. *Atmosphere* **2020**, *11*, 1374. [CrossRef]
68. Phiri, M.; Shiferaw, Y.A.; Tesfamichael, S.G. Modelling the relationship between groundwater depth and NDVI using time series regression with Distributed Lag M. *S. Afr. J. Geomat.* **2018**, *7*, 147–163. [CrossRef]
69. Martínez-de la Torre, A.; Miguez-Macho, G. Groundwater influence on soil moisture memory and land–atmosphere fluxes in the Iberian Peninsula. *Hydrol. Earth Syst. Sci.* **2019**, *23*, 4909–4932. [CrossRef]
70. Lo, M.H.; Famiglietti, J.S. Effect of water table dynamics on land surface hydrologic memory. *J. Geophys. Res. Atmos.* **2010**, *115*. [CrossRef]
71. Kissell, R.; Poserina, J. Chapter 2—Regression Models. In *Optimal Sports Math, Statistics, and Fantasy*; Kissell, R., Poserina, J., Eds.; Academic Press: Chennai, India, 2017; pp. 39–67.
72. Tadych, D.E.; Ford, M.; Colby, B.G.; Condon, L.E. Historical patterns of well drilling and groundwater depth in Arizona considering groundwater regulation and surface water access. *J. Am. Water Resour. Assoc.* **2024**, *60*, 1193–1208. [CrossRef]
73. Bernat, R.F.; Megdal, S.B.; Eden, S. Long-term storage credits: Analyzing market-based transactions to achieve Arizona water policy objectives. *Water* **2020**, *12*, 568. [CrossRef]
74. Carruth, R.L.; Kahler, L.M.; Conway, B.D. *Groundwater-Storage Change and Land-Surface Elevation Change in Tucson Basin and Avra Valley, South-Central Arizona 2003–2016*; No. 2018-5154; US Geological Survey: Reston, VA, USA, 2018.
75. Hanson, R.T.; Anderson, S.R.; Pool, D.R. *Simulation of Ground-Water Flow and Potential Land Subsidence, Avra Valley, Arizona*; No. 4178; US Department of the Interior, US Geological Survey: Reston, VA, USA, 1990; Volume 90.
76. Conway, B.D. Land subsidence and earth fissures in south-central and southern Arizona, USA. *Hydrogeol. J.* **2016**, *24*, 649–655. [CrossRef]
77. U.S. Geological Survey. Land Subsidence in California. Available online: https://www.usgs.gov/centers/land-subsidence-in-california (accessed on 23 February 2025).
78. Park, S.; Hong, S.H.; Cigna, F. Surface Uplift Induced by Groundwater Level Variations Revealed Using MT-InSAR Time-Series Observations. *Remote Sens.* **2025**, *17*, 3875. [CrossRef]
79. Parker, A.L.; Pigois, J.P.; Filmer, M.S.; Featherstone, W.E.; Timms, N.E.; Penna, N.T. Land uplift linked to managed aquifer recharge in the Perth Basin, Australia. *Int. J. Appl. Earth Obs. Geoinf.* **2021**, *105*, 102637. [CrossRef]
80. Kennedy, J.R. *Groundwater-Storage Change in the North Phoenix Aquifer, Arizona, 2020–2023*; No. 2024-5120; US Geological Survey: Reston, VA, USA, 2025.
81. Scanlon, B.R.; Pool, D.R.; Rateb, A.; Conway, B.; Sorensen, K.; Udall, B.; Reedy, R.C. Multidecadal drought impacts on the Lower Colorado Basin with implications for future management. *Commun. Earth Environ.* **2025**, *6*, 214. [CrossRef]
82. Tapia-Villaseñor, E.M.; Shamir, E.; Megdal, S.B.; Petersen-Perlman, J.D. Impacts of variable climate and effluent flows on the transboundary Santa Cruz aquifer. *J. Am. Water Resour. Assoc.* **2020**, *56*, 409–430. [CrossRef]

83. Scott, P.S.; Mac Nish, R.D.; Maddock, T., III. *Effluent Recharge to the Upper Santa Cruz River Floodplain Aquifer, Santa Cruz County, Arizona*; University of Arizona: Tucson, AZ, USA, 1997.
84. Anning, D.W.; Leenhouts, J.M. Conceptual Understanding and Groundwater Quality of the Basin-Fill Aquifer in the Upper Santa Cruz Basin, Arizona. *Natl. Water-Qual. Assess. Program* **2010**, *1781*, 123–144.
85. Williams, S.A.; Zuniga-Teran, A.A.; Megdal, S.B.; Quanrud, D.M.; Christopherson, G. Assessing the Relationship Between Groundwater Availability, Access, and Contamination Risk in Arizona's Drinking Water Sources. *Water* **2025**, *17*, 1097. [CrossRef]
86. Gober, P.; Kirkwood, C.W. Vulnerability assessment of climate-induced water shortage in Phoenix. *Proc. Natl. Acad. Sci. USA* **2010**, *107*, 21295–21299. [CrossRef]
87. Asadollahi, A.; VB, M.K.; Ghimire, A.B.; Poudel, B.; Shin, S. The impact of climate change and urbanization on groundwater levels: A system dynamics model analysis. *Environ. Prot. Res.* **2024**, *4*, 1–15. [CrossRef]

**Disclaimer/Publisher's Note:** The statements, opinions and data contained in all publications are solely those of the individual author(s) and contributor(s) and not of MDPI and/or the editor(s). MDPI and/or the editor(s) disclaim responsibility for any injury to people or property resulting from any ideas, methods, instructions or products referred to in the content.